NUMERICAL INVESTIGATION OF MIXED CONVECTION INSIDE A 3-D *L*-SHAPED CAVITY FILLED WITH HYBRID-NANOFLUIDS IN THE PRESENCE OF A HEATING BLOCK

by

Kamal BOUZID [a*], ***Lahoucine BELARCHE*** [a], ***Btissam ABOURIDA*** [b], ***Ali SIADI*** [a], ***and Soufiane NOUARI*** [a]

[a] Laboratory of Mechanics, Processes, Energy and Environment (LMPEE), National School of Applied Sciences, Ibn Zohr Agadir, Morocco
[b] Faculty of Sciences, Semlalia Marrakech, Marrakech Morocco

Original scientific paper
https://doi.org/10.2298/TSCI230916057B

The objective of this investigation is to explore the various factors affecting the heat exchange characteristics of a heating block that is cooled using hybrid nanofluids. The results from this investigation can be useful to enhance the thermal performance and heat transmission efficiency in the design of thermal engineering equipment. To achieve this, we conducted a (3-D) numerical investigation of mixed convection within an L-cavity filled with hybrid nanofluid. Within this cavity, a heating block is located either on the west wall (Case VB) or on the bottom wall (Case HB). In both cases, cold hybrid nanofluids were introduced at a constant temperature and flowed through a portion of the top wall, while the remaining walls were considered adiabatic. The finite volume method along with the Boussinesq approximation were used to solve the governing equations. The numerical results were presented in the form of iso-lines, global Nusselt numbers, and isotherms for several thermal parameters, including Reynolds numbers, Richardson numbers, and hybrid volume fraction. Our results indicated that for all Richardson numbers and in both configurations, VB and HB, the total Nusselt number increased with increasing Reynolds numbers and volume fraction of particles, except in the case of configuration HB when the volume fraction ($\phi = 0\%$) and the Re ≥ 840, and that when the heated block was repositioned from configuration, HB, to configuration, VB, heat transfer increased significantly by 51.16%. Furthermore, we uncovered intriguing results when comparing the two configurations, VB and HB.

Key words: *hybrid-nanofluids, 3-D L-shaped cavity, finite volume method, mixed convection*

Introduction

Heat transfer is an ongoing concern for scientists and engineers, with new fluid methods receiving a lot of interest. Special focus has recently been accorded to nanofluids among these state-of the art fluids. Its distinctive characteristics, which help to improve efficiency of heat transfer in a variety of industrial uses, are responsible for the increasing use of nanofluids. Important areas like heat exchangers, electronic cooling mechanisms, solar energy technologies, energy storage systems, and nuclear reactors complex heat management systems are all covered by these applications. Nanofluids have surfaced as intriguing candidates with

* Corresponding author, e-mail: kamal.bouzid@edu.mz.ac.ma

the potential to transform heat transfer in these crucial areas because of their distinct qualities and abilities.

Numerous researchers have undertaken the challenging task of investigating mixed convection or natural-convection phenomena within highly dynamic enclosures filled with nanofluids. They have approached this inquiry through a combination of numerical simulations and experimental endeavors. These endeavors are aimed at comprehending the intricate behaviors of nanofluids under the influence of convection, shedding light on the complex interplay between fluid dynamics and thermal transport within such energetic enclosures. Through their collective efforts, these authors have contributed valuable insights to the field of nanofluid dynamics within confined spaces, enriching our understanding of these intricate thermal phenomena. Muhyaddin *et al.* [1] investigated the mixed and natural-convection of a nanoencapsulated phase change material within a cavity featuring an electrical element. The study revealed an optimum value for θ_f, ranging from 0.3-0.5 at lower Rayleigh numbers (10^2), and $\theta_f = 0.5$ at higher Rayleigh numbers (10^4). When the dominant heat transfer mechanism was conduction, the existence of nanocapsules had no significant impact on heat transfer. However, at elevated Rayleigh numbers, an enhancement of up to 13% in the Nusselt number was observed. Interestingly, the rotation of the inner cylinder did not contribute to improving heat transfer at high Rayleigh numbers (10^4). Sheikholeslami *et al.* [2] delved into the topic of enhancing the thermal performance of a linear Fresnel solar system. Their investigation revolved around the utilization of water-borne alumina nanoparticles, ultimately leading them to the conclusion that the integration of nanopowders can indeed improve heat exchange in this system. Sannad *et al.* [3] looked into a 3-D hollow filled with nanofluids deliberate the outcome of the heating block location on natural-convection. The findings demonstrate that the Rayleigh number and the volume fraction have a favorable impact and enhance heat transmission. In addition, comparing the two configurations under consideration, the optimal configuration, from the dynamical and thermal point is the one with the heating block located on the upper wall. Doghmi *et al.* [4] reported a 3-D numerical assessment of the impact of the cove introductory on *mixed* convection. They discovered that increasing the Richardson numbers at the active walls causes the global average Nusselt number to rise, and increasing the inlet opening cross-section at the cold and hot walls causes the heat transfer rate to rise and fall, respectively. In their study Gangawane *et al.* [5] investigated mixed convection within a lid-driven cavity that contained a triangular obstacle with a constant heat flux. The study likely explores how the positioning of the block within the cavity affects heat exchange and fluid patterns. This research contributes to our understanding of the thermal behavior in such configurations.

Nevertheless, nanofluids, characterized as liquid-solid blends featuring nanometric-sized fine materials, whether metallic or non-metallic, cannot ensure optimal heat flow due to the potential limitation of the base liquid. This limitation results from the possibility that the base liquid may not be able to adequately promote ideal heat flow on its own. In light of this challenge, researchers are pushing for the use of hybrid nanofluids, which are a revolutionary development in technology. A hybrid nanofluid is essentially a pure fluid that incorporates the suspension of two or more types of nanoparticles. The introduction of multiple nanoparticles into the fluid matrix imparts enhanced thermo-physical characteristics, resulting in a notable improvement in heat transfer efficiency. Asadi *et al*. [6] investigated the efficiency of MWCNT-Al_2O_3/oil hybrid nanofluids at temperatures ranging from 25-50 °C and nanoparticle volume fractions (from 0.12-1.5%). They studied the consistency of nanofluids. By growing the volume portion of the hybrid nanoparticles in both the turbulent and laminar regimes, thermophysical factors such as the pumping power dynamic viscosity, thermal conductivity, heat transfer efficiency, and Nusselt number within the nanofluid were improved. Regarding their experimental outcomes, they also provided correlations to assume dynamic viscosity and thermal conductivity. In their research, Khalili *et al*. [7] explored an innovative cooling system for PV solar units. This system incorporates a thermo-electric layer, hybrid nanomaterials, and *Y*-shaped fins to enhance cooling efficiency. The study likely presents experimental and numerical simulation. Based on the results, they have improved the cooling performance compared to the conventional methods. They results suggest the potential for increasing energy production and enhancing stability in challenged operational conditions. Rashad *et al*. [8] investigated the (Al_2O_3-Cu) water hybrid nanofluid's MHD assorted convection action in an open void to examine how the Nusselt number of hybrid nanofluid change, they tested three different spots of the adiabatic obstacle and various parameters, such as Reynolds number, varying from 1-200, the Richardson number, ranging from 0.01-20, volume portion of nanoparticles ($0 \leq \phi \leq 4\%$), Hartmann number ($1 \leq \mathrm{Ha} \leq 100$), and other input parameters. They found that the cumulative Hartmann number dropped the heat transmission and reduced the entropy formation. Mehmood *et al*. [9] studied the mixed convection of an (Al-water) nanofluid in a tetragonal absorbent cavity using the Koo-Kleinstreuer-Li model. They results shows the effects of the non-linear mode of the magnetic and radiation field effects. They analyzed that the heat flow increased when the permeability increased. The effect of wall physical possessions on heat transmission is just one of the many factors studied. The mixed convection of a concentrated heat sink/source in a Cu-Al_2O_3-water hybrid nanofluid in a 2-D *L*-shaped crack in the magnetic field's presence was investigated by Armaghani *et al.* [10]. they outcomes demonstrated that when switching among sinks and sources with different heat outputs, the sink with the higher heat output is the one whose heat exchange performance improves the most. When it comes to heat transmission, a magnetic field angle of 180° is optimal. Samrat *et al*. [11] conducted an investigation into the MHD mixed convective flow of a hybrid nanofluid within a wavy-walled enclosure. Their findings indicate that altering the concentration of the Cu-Al_2O_3-water hybrid nanofluid, ϕ_{hnp}, from 1% to 4% results in a 7.46% enhancement in the average Nusselt number for Case I and a 5.09% improvement for Case II. Conversely, the average Sherwood number experiences a reduction of 2.42% and 1.58% for Cases I and II, respectively. Moreover, the study emphasizes the significant influence of heating areas and the angle γ on the flow topology, as well as thermal and solutal transport within the wavy enclosure.

Even though there have been many studies on *mixed convection* in craters with various designs and boundary conditions, few of them have looked specifically at the case of mixed convection inside an *L*-shaped cavity with a heating block. Most of the studies that have been done so have used a 2-D approach, which is insufficient for understanding the intricate fluid-flow and heat transfer characteristics within the system. The goal of creating an optimal geometrical model that maximizes the effectiveness of heat transfer while taking into account various scenarios under various flow and temperature conditions is greatly advanced by this work. The outcomes of this research hold considerable promise in advancing the comprehension of mixed convection within intricate geometries, offering insights that can be leveraged to augment thermal performance and optimize heat transmission efficiency in the design of thermal engineering equipment, including heat exchangers and related systems.

Problem formulation

Figure 1 illustrates a purposefully designed set-up (3*H*) with specific configuration and co-ordinates. This set-up comprises a 3-D *L*-shaped cavity characterized by an inlet opening with a cross-section width ($w = H/4$) positioned on the upper part of the left horizontal wall, the inlet opening serves as the entry point for the hybrid nanofluid, which enters with a cold temperature, T_c, and a uniform velocity, V_{in}. The fluid is subsequently expelled through an opening located at the bottom of the right vertical wall, with a relative height ($w = H/4$).

In the initial configuration denoted as, VB, a heated block characterized by dimensions ($b = H/5$) and ($a = 3w/5$) is placed along the left wall, precisely at a height indicated by ($h = H/4$). Conversely, in the second configuration denoted, HB, an identical heated block with dimensions ($b = H/5$) and ($a = 3w/5$) is positioned at the base of the cavity, specifically at ($h = H/4$). In both configurations, these heated blocks are strategically located at the center of the cavity, precisely with a width corresponding to ($l = H/2$). Within both set-ups, all remaining walls are treated as adiabatic surfaces, with no heat exchange occurring.

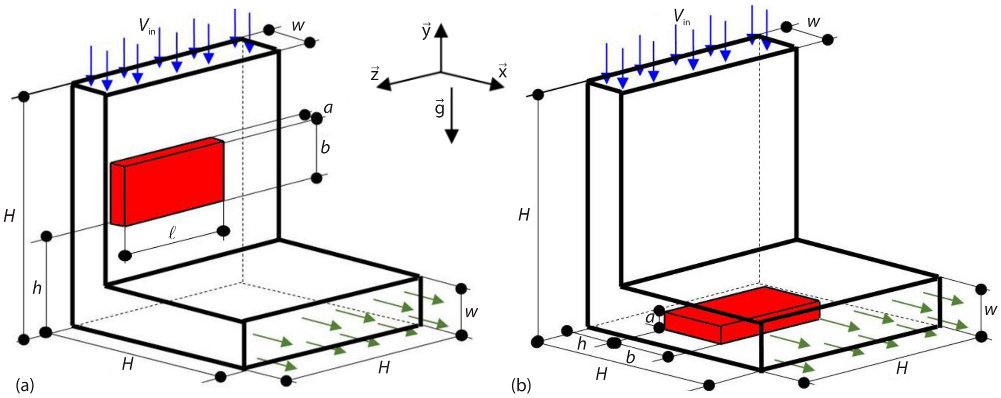

Figure 1. Studied configurations and co-ordinates; (a) VB configuration and (b) HB configuration

Numerical scheme and mathematical modelling

As depicted in fig. 1, our investigation delves into the intricacies of mixed convection flow within a 3-D enclosure containing a composite nanofluid comprised of (Cu, Al_2O_3 and water) which provide the complementary qualities of aluminum's lightweight design and copper's high heat conductivity. Because of its high electrical and thermal conductivity, copper facilitates effective heat dissipation, and aluminum's low weight helps to keep the hybrid-nanofluid's total weight to a minimum. In our analysis, we have made several fundamental assumptions to simplify the scenario. Firstly, we assume that the flow is unidirectional and incompressible, spanning three spatial dimensions. Additionally, we neglect radiative effects and consider the fluid behavior to be Newtonian. Furthermore, to describe the density variations within the fluid, we employ the Boussinesq approximation, which simplifies the density variation due to temperature rather than considering the full spectrum of fluid property variations. Table 1 displays a comprehensive understanding of our chosen thermo-physical properties for both the nanomaterials and the base fluid.

Under these aforementioned assumptions, the governing equations that dictate the flow behavior are defined, as presented by [10]. These equations form the foundation of our analysis and guide our exploration into mixed convection flow within the hybrid-nanofluid-filled enclosure:

$$\frac{\partial u}{\partial x}+\frac{\partial w}{\partial y}+\frac{\partial v}{\partial z}=0 \tag{1}$$

$$\frac{\partial(uu)}{\partial x}+\frac{\partial(vu)}{\partial y}+\frac{\partial(wu)}{\partial z}=-\frac{1}{\rho_{\text{hnf}}}\frac{\partial p}{\partial x}+\nu_{\text{hnf}}\left(\frac{\partial^2 u}{\partial x^2}+\frac{\partial^2 u}{\partial y^2}+\frac{\partial^2 u}{\partial z^2}\right) \tag{2}$$

$$\frac{\partial(uv)}{\partial x}+\frac{\partial(vv)}{\partial y}+\frac{\partial(wv)}{\partial z}=-\frac{1}{\rho_{\text{hnf}}}\frac{\partial p}{\partial y}+\nu_{\text{hnf}}\left(\frac{\partial^2 v}{\partial x^2}+\frac{\partial^2 v}{\partial y^2}+\frac{\partial^2 v}{\partial z^2}\right)+\frac{(\rho\beta)_{\text{hnf}}}{\rho_{\text{hnf}}}\text{g}(T=T_{\text{ref}}) \tag{3}$$

$$\frac{\partial(uw)}{\partial x}+\frac{\partial(vw)}{\partial y}+\frac{\partial(ww)}{\partial z}=-\frac{1}{\rho_{\text{hnf}}}\frac{\partial p}{\partial z}+\nu_{\text{hnf}}\left(\frac{\partial^2 w}{\partial x^2}+\frac{\partial^2 w}{\partial y^2}+\frac{\partial^2 w}{\partial z^2}\right) \tag{4}$$

$$\frac{\partial(uT)}{\partial x}+\frac{\partial(vT)}{\partial y}+\frac{\partial(wT)}{\partial z}=\alpha_{\text{hnf}}\left(\frac{\partial^2 T}{\partial x^2}+\frac{\partial^2 T}{\partial y^2}+\frac{\partial^2 T}{\partial z^2}\right) \tag{5}$$

Table 1. Properties of hybrid-nanofluids [16]

Property	Water	Cu	Al_2O_3
ρ [kgm^{-3}]	997.1	8933	3970
k [Wm^{-1}K^{-1}]	0.613	401	40
β [K^{-1}]	$21\cdot10^{5}$	$1.67\cdot10^{-5}$	$0.85\cdot10^{-5}$
C_p [Jkg^{-1}K^{-1}]	4179	385	765

The boundary conditions:

– At the outlet

$$\frac{\partial u}{\partial x}=0\ ,\ \frac{\partial v}{\partial y}=0,\ \frac{\partial w}{\partial z}=0,\ \frac{\partial T}{\partial n}=0$$

– At the creek

$$v=v_{\text{in}},\quad u=w_0,\quad T=T_{\text{c}}$$

– On the remaining walls

$$u=v=w=0,\ \frac{\partial T}{\partial m}=0$$

where m is the normal track to the considered wall.

– At the block

$$\frac{\partial T}{\partial m'}=-\frac{q''}{k_{\text{hnf}}},\ u=v=w=0$$

where n' is the normal direction the block wall.

The properties of the hybrid-nanofluid are specified by the succeeding equations.

The equivalent density of the hybrid nanofluid:

$$\rho_{\text{hnf}}=\phi_{\text{p1}}\rho_{\text{p1}}+\phi_{\text{p2}}\rho_{\text{p2}}+(1-\phi)\rho_{\text{f}} \tag{6}$$

The equivalent concentration of two nanoparticles is given:

$$\phi=\phi_{\text{p1}}+\phi_{\text{p2}} \tag{7}$$

The equivalent heat capacitance is determined:

$$(\rho C_p)_{\text{hnf}}=\phi_{\text{p1}}(\rho C_p)_{\text{p1}}+\phi_{\text{p2}}(\rho C_{\text{p}})_{\text{p2}}+(1-\phi)(\rho C_p)_{\text{f}} \tag{8}$$

The coefficient thermal expansion is given:

$$(\rho\beta)_{\text{hnf}} = \phi_{\text{p1}}(\rho\beta)_{\text{p1}} + \phi_{\text{p2}}(\rho\beta)_{\text{p2}} + (1-\phi)(\rho\beta)_{\text{f}} \tag{9}$$

Hybrid nanofluid having the thermal diffusivity:

$$\alpha_{\text{hnf}} = \frac{k_{\text{hnf}}}{(\rho C_p)_{\text{hnf}}} \tag{10}$$

Determination of The thermal conductivity:

$$\frac{k_{\text{hnf}}}{k_{\text{f}}} = \frac{\dfrac{(\phi_{\text{p1}}k_{\text{p1}} + \phi_{\text{p2}}k_{\text{p2}})}{\phi} + 2k_{\text{f}} + 2(\phi_{\text{p1}}k_{\text{p1}} + \phi_{\text{p2}}k_{\text{p2}}) - 2\phi k_{\text{f}}}{\dfrac{(\phi_{\text{p1}}k_{\text{p1}} + \phi_{\text{p2}}k_{\text{p2}})}{\phi} - (\phi_{\text{p1}}k_{\text{p1}} + \phi_{\text{p2}}k_{\text{p2}}) + 2k_{\text{f}} + \phi k_{\text{f}}} \tag{11}$$

The form of dynamic viscosity of the hybrid nanofluid is expressed:

$$\mu_{\text{hnf}} = \frac{\mu_{\text{f}}}{\left[1-(\phi_{\text{p1}}+\phi_{\text{p2}})\right]^{2.5}} \tag{12}$$

Seeing the boundaries:

$$X = \frac{x}{H},\ Z = \frac{z}{H},\ y = \frac{y}{H},\ U = \frac{u}{V_{\text{in}}},\ W = \frac{w}{V_{\text{in}}},\ V = \frac{v}{V_{\text{in}}},\ \theta = \frac{T - T_{\text{c}}}{q''H}k_{\text{hnf}},\ \text{and}\ P = \frac{p}{\rho_{\text{hnf}} f V_{\text{in}}^2} \tag{13}$$

The governing equations become the following dimensionless ones:

$$\frac{\partial U}{\partial X} + \frac{\partial V}{\partial Y} + \frac{\partial W}{\partial Z} = 0 \tag{14}$$

$$U\frac{\partial(U)}{\partial X} + U\frac{\partial(V)}{\partial Y} + U\frac{\partial(W)}{\partial Z} = -\frac{\partial P}{\partial X} + \frac{1}{\text{Re}}\left(\frac{\nu_{\text{hnf}}}{\nu_{\text{f}}}\right)\left(\frac{\partial^2 U}{\partial X^2} + \frac{\partial^2 U}{\partial Y^2} + \frac{\partial^2 U}{\partial Z^2}\right) \tag{15}$$

$$V\frac{\partial(U)}{\partial X} + V\frac{\partial(W)}{\partial Z} + V\frac{\partial(V)}{\partial Y} = -\frac{\partial P}{\partial Y} + \frac{1}{\text{Re}}\left(\frac{\nu_{\text{hnf}}}{\nu_{\text{f}}}\right)\left(\frac{\partial^2 V}{\partial X^2} + \frac{\partial^2 V}{\partial Y^2} + \frac{\partial^2 V}{\partial Z^2}\right) + \text{Ri}\frac{(\rho\beta)_{\text{hnf}}}{\rho_{\text{nf}}\beta_{\text{f}}}\theta \tag{16}$$

$$W\frac{\partial(U)}{\partial X} + W\frac{\partial(V)}{\partial Y} + W\frac{\partial(W)}{\partial Z} = -\frac{\partial P}{\partial Z} + \frac{1}{\text{Re}}\left(\frac{\nu_{\text{hnf}}}{\nu_{\text{f}}}\right)\left(\frac{\partial^2 W}{\partial X^2} + \frac{\partial^2 W}{\partial Y^2} + \frac{\partial^2 W}{\partial Z^2}\right) \tag{17}$$

$$U\frac{\partial\theta}{\partial X} + V\frac{\partial\theta}{\partial Y} + W\frac{\partial\theta}{\partial Z} = \left(\frac{1}{\text{RePr}}\right)\left(\frac{\alpha_{\text{hnf}}}{\alpha_{\text{f}}}\right)\left(\frac{\partial^2\theta}{\partial X^2} + \frac{\partial^2\theta}{\partial Y^2} + \frac{\partial^2\theta}{\partial Z^2}\right) \tag{18}$$

where

$$\text{Ri} = \frac{\text{Gr}}{\text{Re}},\ \text{Re} = \frac{V_{\text{in}}H}{\nu_{\text{f}}},\ \text{Pr} = \frac{\nu_{\text{f}}}{\alpha_{\text{f}}},\ \text{and}\ \text{Gr} = \frac{g\beta_{\text{f}}H^3\Delta T}{\nu_{\text{f}}^{\ 2}}$$

are, respectively Richardson, Reynolds, Prandtl, and Grashof numbers.

The non-dimensional boundary conditions:

– At the outlet

$$\frac{\partial U}{\partial X} = 0,\ \frac{\partial W}{\partial Z} = 0,\ \frac{\partial V}{\partial Y} = 0,\ \frac{\partial\theta}{\partial n} = 0$$

– At the inlet

$$V = V_{\text{in}},\ W = U = 0,\ \theta = 0$$

– On the remaining walls

$$U = V = W = 0,\ \frac{\partial \theta}{\partial m} = 0$$

where m is the usual direction the wall.

– At the block

$$\frac{\partial \theta}{\partial m'} = -\frac{k_{\text{hnf}}}{k_{\text{f}}},\ U = V = W = 0$$

where m' is the normal direction the block wall.

Depending on the considered configuration, the Nusselt number is given:

– For VB configuration

The local Nusselt number, on the five sections (S_1-S_5) of the vertical block, is given:

$$\begin{aligned}
\text{Nu}_{\text{VS1}} &= \frac{q''H}{[T(x,z)_{y=h} - T_C]k} = \frac{1}{\theta(X,Z)_{Y=h}} \\
\text{Nu}_{\text{VS2}} &= \frac{q''H}{[T(x,z)_{y=h+b} - T_C]k} = \frac{1}{\theta(X,Z)_{Y=h+B}} \\
\text{Nu}_{\text{VS3}} &= \frac{q''H}{[T(x,z)_{x=a} - T_C]k} = \frac{1}{\theta(X,Z)_{X=A}} \\
\text{Nu}_{\text{VS4}} &= \frac{q''H}{[T(x,y)_{z=H/4} - T_C]k} = \frac{1}{\theta(X,Y)_{Z=H/4}} \\
\text{Nu}_{\text{VS5}} &= \frac{q''H}{[T(x,y)_{y=3H/4} - T_C]k} = \frac{1}{\theta(X,Y)_{Z=3H/4}}
\end{aligned} \tag{19}$$

The global Nusselt number is typically described:

$$\text{Nu}_{\text{VG}} = \text{Nu}_{\text{VSG1}} + \text{Nu}_{\text{VSG2}} + \text{Nu}_{\text{VSG3}} + \text{Nu}_{\text{VSG4}} + \text{Nu}_{\text{VSG5}} \tag{20}$$

where Nu_{VSGi}, are the average Nusselt numbers for each section:

$$\begin{aligned}
\text{Nu}_{\text{VSG1}} &= \frac{2}{A \times H} \int_{H/4}^{3H/4} \int_0^A \text{Nu}_{\text{VS1}} \text{d}X\text{d}Z \\
\text{Nu}_{\text{VSG2}} &= \frac{2}{A \times H} \int_{H/4}^{3H/4} \int_0^A \text{Nu}_{\text{VSG2}} \text{d}X\text{d}Z \\
\text{Nu}_{\text{VSG3}} &= \frac{2}{B \times H} \int_0^B \int_{H/4}^{3H/4} \text{Nu}_{\text{VSG3}} \text{d}Y\text{d}Z \\
\text{Nu}_{\text{VSG4}} &= \frac{1}{B \times A} \int_H^{H+B} \int_0^A \text{Nu}_{\text{VSG4}} \text{d}Y\text{d}X \\
\text{Nu}_{\text{VSG5}} &= \frac{1}{B \times A} \int_H^{H+B} \int_0^A \text{Nu}_{\text{VSG5}} \text{d}Y\text{d}X
\end{aligned} \tag{21}$$

– For HB configuration:

The local Nusselt number, on the five sections (S_1-S_5) of the horizontal block:

$$\begin{aligned}
\mathrm{Nu}_{\mathrm{HS1}} &= \frac{q''H}{[T(y,z)_{x=h} - T_\mathrm{c}]k} = \frac{1}{\theta(Y,Z)_{X=h}} \\
\mathrm{Nu}_{\mathrm{HS2}} &= \frac{q''H}{[T(y,z)_{x=h+b} - T_\mathrm{c}]k} = \frac{1}{\theta(Y,Z)_{X=h+B}} \\
\mathrm{Nu}_{\mathrm{HS3}} &= \frac{q''H}{[T(x,z)_{y=a} - T_\mathrm{c}]k} = \frac{1}{\theta(X,Z)_{Y=A}} \\
\mathrm{Nu}_{\mathrm{HS4}} &= \frac{q''H}{[T(x,y)_{z=H/4} - T_\mathrm{c}]k} = \frac{1}{\theta(X,Y)_{Z=H/4}} \\
\mathrm{Nu}_{\mathrm{HS5}} &= \frac{q''H}{[T(x,y)_{z=3H/4} - T_\mathrm{c}]k} = \frac{1}{\theta(X,Y)_{Z=3H/4}}
\end{aligned} \tag{22}$$

and the global Nusselt number is defined:

$$\mathrm{Nu}_{\mathrm{HG}} = \mathrm{Nu}_{\mathrm{HSG1}} + \mathrm{Nu}_{\mathrm{HSG2}} + \mathrm{Nu}_{\mathrm{HSG3}} + \mathrm{Nu}_{\mathrm{HSG4}} + \mathrm{Nu}_{\mathrm{HSG5}} \tag{23}$$

Where $\mathrm{Nu}_{\mathrm{HSG}i}$, are the average Nusselt numbers for each sections:

$$\begin{aligned}
\mathrm{Nu}_{\mathrm{HSG1}} &= \frac{2}{A\times H}\int_{H/4}^{3H/4}\int_0^A \mathrm{Nu}_{\mathrm{HS1}}\mathrm{d}Y\mathrm{d}Z \\
\mathrm{Nu}_{\mathrm{HSG2}} &= \frac{2}{A\times H}\int_{H/4}^{3H/4}\int_0^A \mathrm{Nu}_{\mathrm{HS2}}\mathrm{d}Y\mathrm{d}Z \\
\mathrm{Nu}_{\mathrm{HSG3}} &= \frac{2}{B\times H}\int_0^B\int_{H/4}^{3H/4} \mathrm{Nu}_{\mathrm{HS3}}\mathrm{d}X\mathrm{d}Z \\
\mathrm{Nu}_{\mathrm{HSG4}} &= \frac{1}{B\times A}\int_H^{H+B}\int_0^A \mathrm{Nu}_{\mathrm{HS4}}\mathrm{d}Y\mathrm{d}X \\
\mathrm{Nu}_{\mathrm{HSG5}} &= \frac{1}{B\times A}\int_H^{H+B}\int_0^A \mathrm{Nu}_{\mathrm{HS5}}\mathrm{d}Y\mathrm{d}X
\end{aligned} \tag{24}$$

Numerical method

We employed a custom-developed FORTRAN code to effectively address the mathematical model. To capture the underlying physics, we discretized both the energy equations and the Navier-Stokes equations employing the finite volume method, a technique initially formulated by Patankar [12]. This method incorporates a power law scheme to handle the convective elements within the equations, ensuring an accurate representation of the fluid dynamics.

To solve the resulting algebraic equations, we implemented the tridiagonal matrix algorithm, which iteratively tackles the system of equations. This iterative approach aids in efficiently converging towards a solution.

The convergence of our numerical code was rigorously assessed, and this assessment hinged on specific criteria that were meticulously defined and adhered to throughout the computational process:

$$\sum_{i,j,k=1}^{i\max, j\max, k\max} \frac{\left|\Phi_{i,j,k}^{n+1} - \Phi_{i,j,k}^{n}\right|}{\left|\Phi_{i,j,k}^{n}\right|} \le 10^{-5} \tag{25}$$

where Φ is the dependent variable P, W, V, U, and T, n – the iteration number, and the directories i, j, and k show the grating locations.

Grid size independency

The selection of an appropriate grid size plays a crucial role in computational simulations, influencing both accuracy and computational resources. To establish grid independence for the solution, the Nusselt number was assessed using various uniform grid sizes, and the results are detailed in tab. 2. Through this analysis, it was determined that a grid size of 71×71×71 was well-suited for the current study, striking a balance between result accuracy and computational cost.

Moreover, refining the grid to 91×91×91 showed only a marginal difference within 1.18%. This indicates that the adjustment in grid size did not significantly affect the overall system performance, reinforcing the suitability of the 71×71×71 grid for the research objectives. The findings of this investigation validate the chosen grid size, instilling confidence in the accuracy of the outcomes achieved while enhancing computational efficiency.

Table 2. Grid size tests

Grid Size	41×41×41	61×61×61	71×71×71	81×81×81	91×91×91
Nusselt number	44.18	55.28	58.99	59.40	60.11

Code validation

We thoroughly compared our findings with those of previous research in order to confirm the accuracy of our numerical code. The Nusselt numbers that were acquired were compared to the results of Ravnik [13] and Iwatsu *et al.* [14] for a range of Rayleigh numbers, and the results are methodically displayed in tabs. 3 and 4. Furthermore, as shown in fig. 2, we evaluated the temperature distribution by contrasting our findings with those published by Iwatsu *et al.* [14] and Khanafer and Chamkha [15].

With a maximum difference of less than 3.24%, the careful comparison with the works of Ravnik [13], Iwatsu *et al.* [14], and Chamkha and Khanafer [15] reveals a commendable agreement. The precise agreement demonstrates the validity of our findings and the robustness of our computational approach in displaying the nuances of the thermal phenomena under study. It also highlights the accuracy and dependability of our numerical code.

Table 3. Comparison of Nusselt number with those of [13]

Rayleigh number	Water		Difference	Water + Cu $\phi = 0.1$		Difference	Water + Al_2O_3 $\phi = 0.1$		Difference
	Present work	[13]		Present work	[13]		Present work	[13]	
10^3	1.082	1.071	1.02%	1.381	1.363	1.32%	1.362	1.345	1.26%
10^4	2.114	2.078	1.73%	2.257	2.237	0.89%	2.187	2.168	0.87%
10^5	4.631	4.510	2.68%	5.047	4.946	2.04%	4.904	4.806	2.03%
10^6	9.325	9.032	3.24%	10.38	10.08	2.97%	10.09	9.817	2.78%

Table 4. Comparison of Nusselt number with those of [14]

Reynolds number	Gr = 10^2		Difference	Gr = 10^4		Difference	Gr = 10^6		Difference
	Present work	[14]		Present work	[14]		Present work	[14]	
10^2	1.9	1.94	2.06%	1.36	1.34	1.49%	1.03	1.02	0.98%
400	3.88	3.84	1.04%	3.63	3.62	0.28%	1.21	1.22	0.82%
10^3	6.5	6.33	2.69%	6.32	6.29	0.48%	1.75	1.77	1.13%

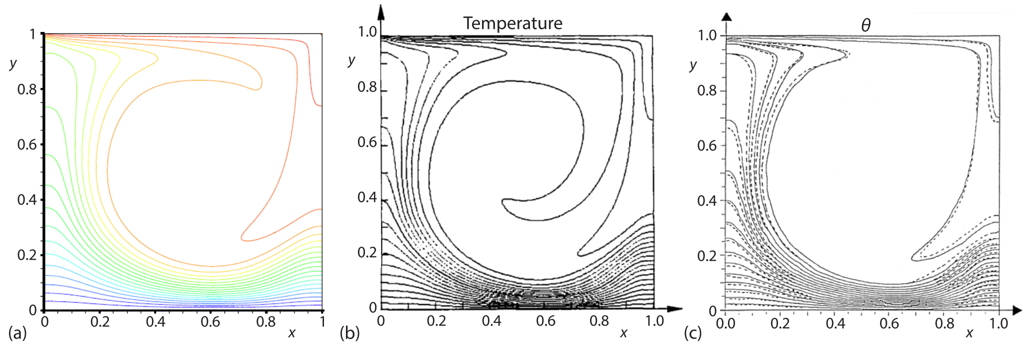

Figure 2. Comparison of the isotherm reported at Z = 0.5 plane, with those of [14] and [15]; (a) currend data, (b) [14], and (c) [15]

Results and discussion

The goal of the current work is to study the impact of geometrical and thermal parameters on fluid-flow phenomena and heat transfer in a 3-D L-shaped crater. The global Nusselt number, streamlines, temperature distribution and flow fields are examined in the two configurations: VB and HB, and through a wide range of thermal parameters: Richardson numbers ($0.1 \leq \mathrm{Ri} \leq 10$), Reynolds numbers ($10 \leq \mathrm{Re} \leq 1900$), and volume fraction of nanoparticles ($0\% \leq \phi \leq 4\%$).

Effect of the thermal parameters

The examination of the isotherms in different planes for the two configurations (VB and HB) is shown in fig. 3. When the plane Z = 0.5, the cavity displayed excellent symmetry. This occurs because of the symmetry of the geometry and thermal boundary conditions. Compared to the other planes, the Z = 0.5 plane shows higher activity and seems to be sufficient for representing the dynamical and thermal fields in the L-shaped cavity.

TheVB configuration

Initially, our focus was on exploring the configuration involving the placement of the heating block on the west wall (referred to as VB). In fig. 4, the thermal fields and streamlines are visually represented, considering a constant Richardson number (Ri = 0.1). The investigation encompasses a range of Reynolds numbers (Re = 100, 700, 1500) and various volume fractions (ϕ = 0%, 2%, 4%). This comprehensive analysis provides insights into the fluid dynamics under these specified conditions.

At Reynolds number (Re = 100) and with a volume fraction, ϕ, of 0%, the flow exhibits a subdued character. The distinct lines maintain a relatively consistent configuration,

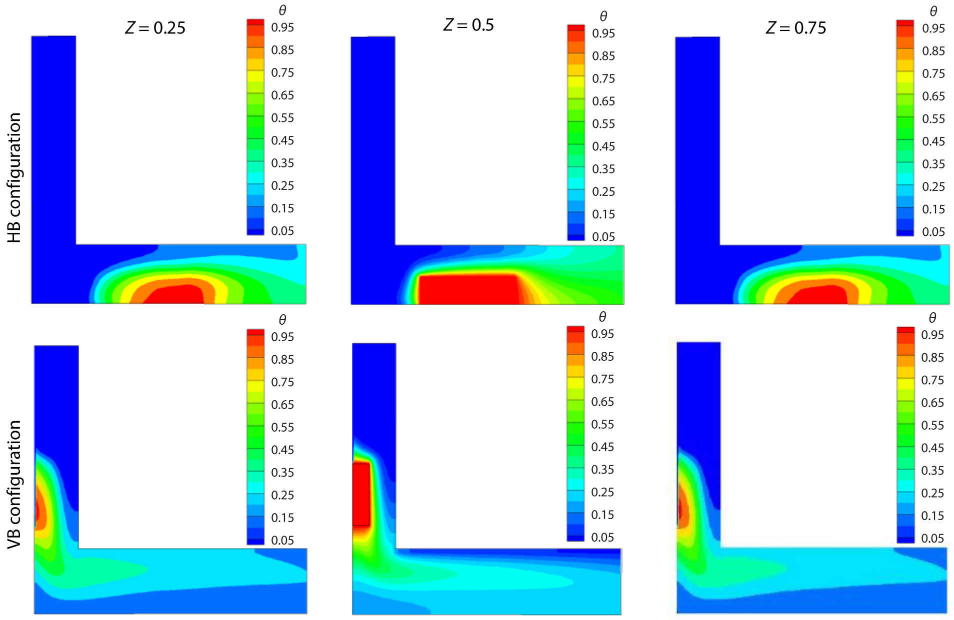

Figure 3. Temperature distribution for the HB and VB configurations at various Z positions (0.25, 0.5 and 0.75), for Re = 800, Ri = 0.1 and ϕ = 3%; (a) Z = 0.25, (b), Z = 0.5, and (c) Z = 0.75

preserving their shape from the upper extremity of the block to the lower region of the cavity, with minimal deviation observed at both ends. Notably, the isotherms highlight a uniform concentration of high temperature zones in close proximity to the heating block, emphasizing the localized nature of elevated temperatures within this particular configuration.

Furthermore, with a rise in the Reynolds number to Re = 700, there is a notable growth in the redirection of the fluid as it interacts with the bottom of the hollow. The corresponding isotherms exhibit a stratified and concentrated pattern encircling the heating block. Within the remaining regions of the crater, the isotherm lines associated with lower and middle temperatures scurry parallel to each other, indicating a distinct thermal behavior in these sections. This heightened Reynolds number introduces intricate fluid dynamics, influencing both the redirection patterns and the temperature distribution within the examined configuration.

With a further increase in the Reynolds number to Re = 1500, a pronounced intensification in inflow strength is observed. The streamlines vividly depict the heightened redirection of the fluid along the bottom of the hollow, extending all the way up to the top of the exit. Examining the heat transmission rate within the hollow, it is noteworthy that lower values are correlated with the isotherms. These isotherms align in the direction of the outlet, indicating a distinct heat distribution pattern within the system. The augmentation of the Reynolds number to 1500 significantly influences both the fluid dynamics and the thermal characteristics, showcasing a more robust and intricate flow pattern.

Upon elevating the volume fraction of hybrid nanofluid particles to ϕ = 2% at Reynolds number Re = 100, the increase in heat transfer is not substantial when compared to ϕ = 0%. Clearly, the incorporation of metal nanoparticles into the base fluid, coupled with their interaction with the incoming flow and the heated block, proves insufficient to induce significant alterations in fluid density and particle mobility.

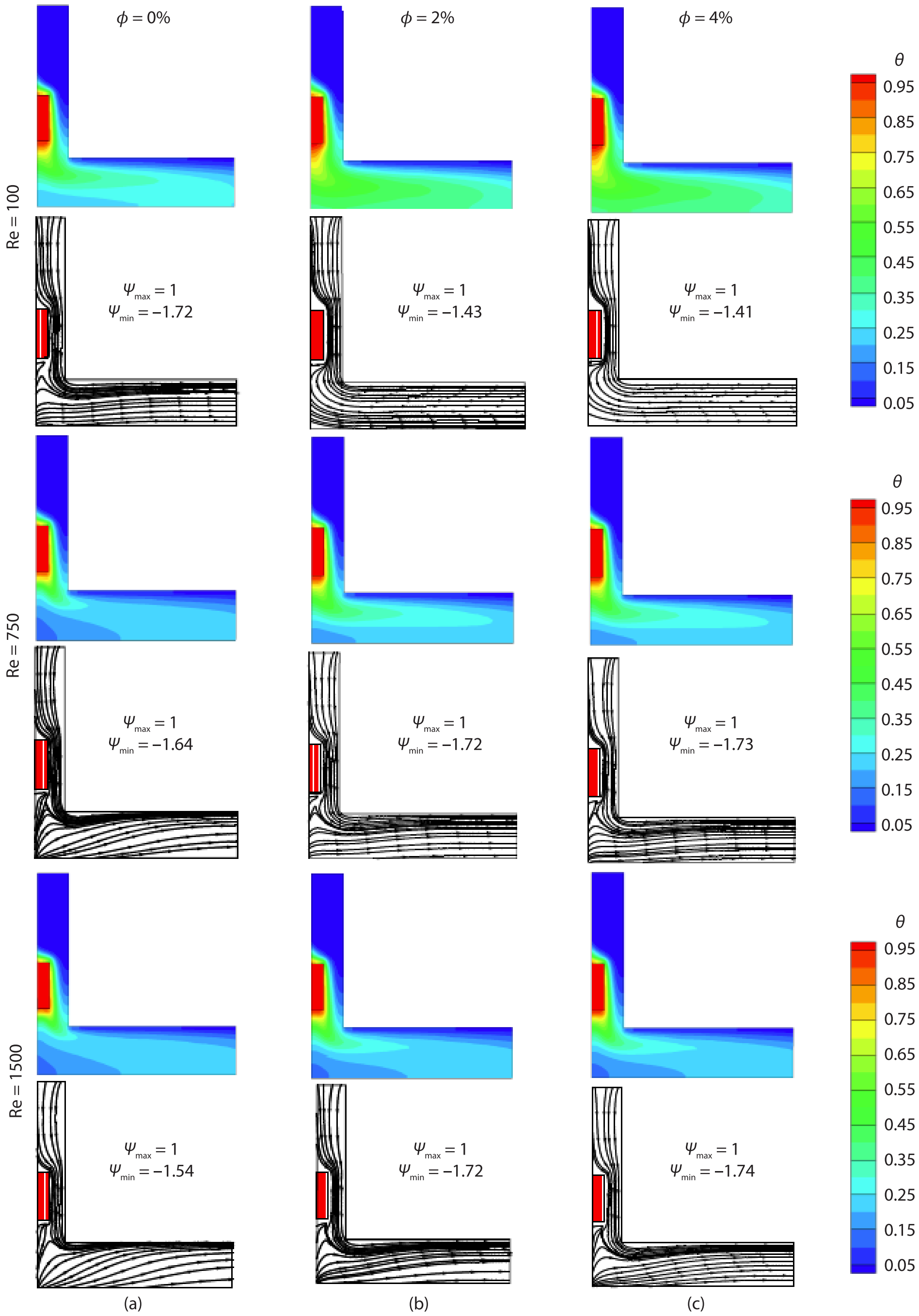

Figure 4. Isotherm lines (up) and streamlines (down) at Z = 0.5 in the case VB configuration, for Ri = 0.1, for various volumesfractionof nanoparticles (0%, 2%, 4%), for various Reynolds numbers Re = 100, 750, and 1500; (a) ϕ = 0%, (b) ϕ = 2%, and (c) ϕ = 4%

However, an impressive enhancement in heat transfer is witnessed with a subsequent increase in the Reynolds number to 700. Concurrently, the fluid velocity experiences a significant surge. This phenomenon is attributed to the delicate equilibrium between inertial forces and nanoparticle characteristics. The flow field is notably characterized by the formation of a minute anti-clockwise vortex beneath the block as the Reynolds number attains Re = 1500. In comparison Re = 700, this leads to a substantial augmentation in heat transfer exchange, underscoring the intricate interplay between fluid dynamics and nanoparticle behavior in this heightened Reynolds number regime.

Upon setting the volume fraction of nanoparticles to (ϕ = 4%), a comparable behavior to ϕ = 2% is discerned in both the isotherm lines and streamlines, accompanied by a notable increase in the heat transfer rate across all Reynolds number values. This heightened heat transfer is attributed to the substantial impact of the interaction between the flowing fluid and the heated block, playing a pivotal role in altering the fluid's density and inducing particle motion.

Notably, the temperature distribution becomes concentrated around the heated block as Reynolds numbers reach elevated values and gradually shifts towards the hollow exit. This observed shift is a consequence of the interaction between the incoming cold flow and the buoyancy effect generated by the heated block. The intricate dynamics between the fluid, nanoparticle behavior, and thermal effects contribute to a nuanced temperature distribution pattern within the system.

Upon augmenting the volume fraction of hybrid nanofluid particles to (ϕ = 4%) at a Reynolds number of Re = 100, the heat transfer observed was comparatively lower than that of pure water. However, as the Reynolds number was increased to Re = 700, a convective circulation cell manifested on the right side of the heated block, progressively expanding in size with further increases in the Reynolds number. The unobstructed lines representing external flow demonstrated a discernible impact on the heated surface of the block, indicating an enhanced heat transfer performance for elevated Reynolds numbers. This suggests a complex interplay between nanoparticle concentration and Reynolds number, influencing the convective circulation and subsequently affecting heat transfer dynamics within the system.

The HB configuration

In order to assess the heat performance and flow structures relative to the preceding case (VB), we present the streamlines and isotherms within the Z = 0.5 plane for the (HB) configuration. In this arrangement, the heating block is strategically positioned at the bottommost part of the cavity, as illustrated in fig. 5. This investigation aims to provide a comparative analysis of the thermal and fluid dynamic characteristics in the (HB) arrangement.

Several simulations were conducted, spanning a range of Reynolds numbers ($10 \leq \mathrm{Re} \leq 1500$), while maintaining a consistent Richardson number (Ri = 0.1). These simulations encompass various scenarios, considering both pure water (ϕ = 0%) and hybrid nanofluids with different volume fractions (ϕ = 2% and ϕ = 4%).

With a nanoparticle volume fraction of (ϕ = 0%) and at a Reynolds number of Re = 100, the unobstructed lines representing external forced movement effectively covered the entire left side of the block, creating a swirling vortex on the right side of the heated block as they approached the exit. The introduction of the Reynolds number at Re = 700 leads to a substantial augmentation in both the size of the vortex and thermal transfer. Contrastingly, when the Reynolds number was further increased to Re = 1500, there was a noticeable decrease in the heat flow rate despite the intensified fluid dynamics. This intriguing observation suggests a non-linear relationship between Reynolds number and heat transfer under the specified conditions.

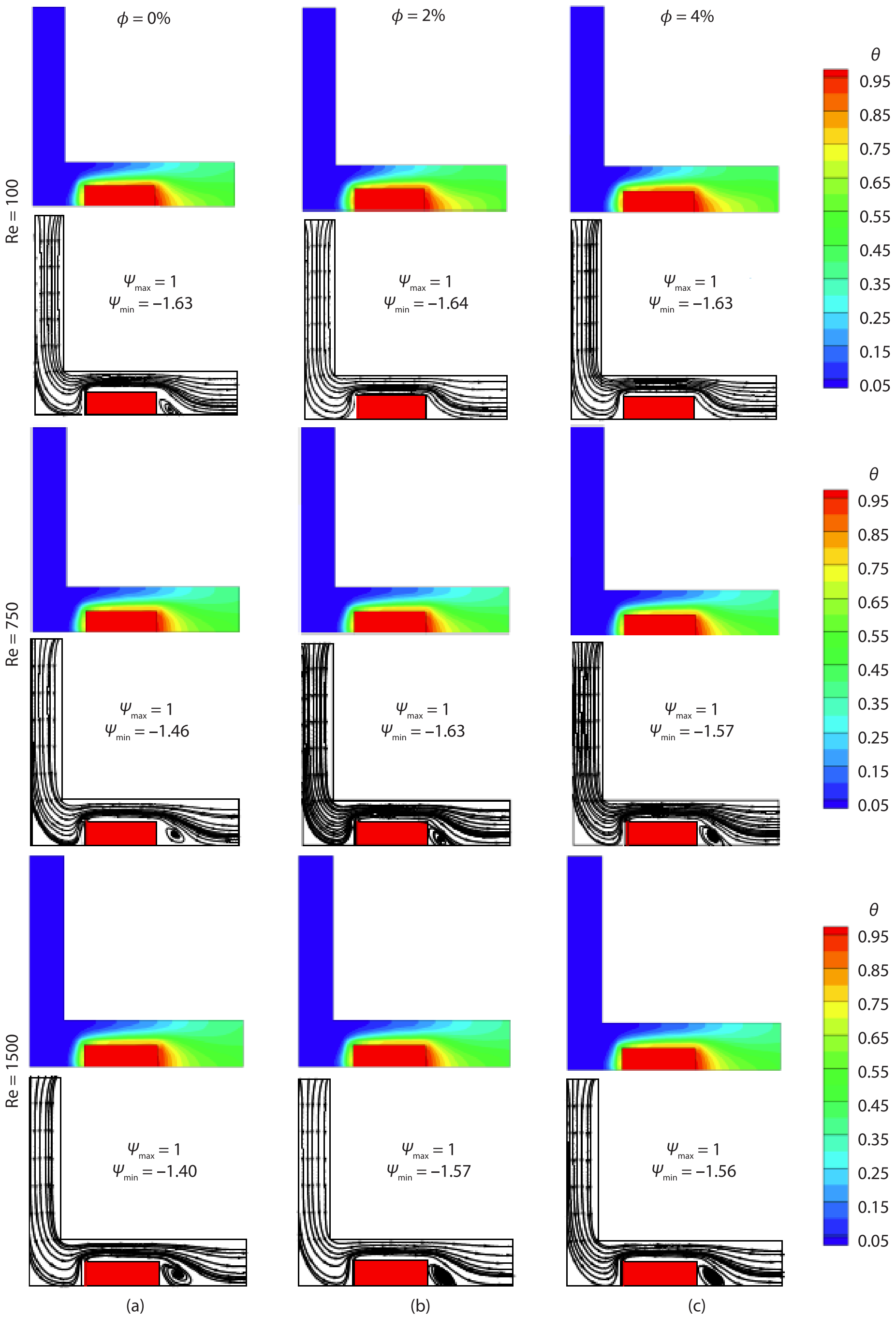

Figure 5. Isotherm lines (up) and streamlines (down) at Z = 0.5 in the case HB configuration, for Ri = 0.1, for various volumes fraction of nanoparticles (0%, 2%, 4%), for various Reynolds numbers Re = 100, 750, and 1500; (a) ϕ = 0%, (b) ϕ = 2%, and (c) ϕ = 4%

Upon elevating the volume fraction of hybrid nanofluid particles to (ϕ = 2%) at a Reynolds number of Re = 100, the previously observed counter-clockwise vortex on the right side of the heated block, noticeable at (ϕ = 0%), vanishes. This disappearance can be attributed to the interaction between metal nanoparticles in the base liquid and the incoming flow, leading to changes in fluid density and particle mobility.

Upon further increasing the Reynolds number to Re = 700, the flow lines reveal the presence of a vortex cell to the right of the heated block. Subsequently, at Re = 1500, this vortex cell above the heated block grows in size, indicative of the increasing influence of inertial effects. The enclosure illustrates isotherm lines corresponding to lower temperatures that run parallel to the heated block, portraying a symmetrical pattern. Conversely, the isotherms around the flow oriented heated block exhibit asymmetry. This behavior is reminiscent of pure conductive heat transfer.

Additionally, as the Reynolds number increases, there is a stimulation of the expansion of the cold zone, leading to a noticeable tightening of the fronts towards the left end of the block. This observation highlights the intricate interplay between nanoparticle concentration, Reynolds number, and fluid dynamics, contributing to the evolving thermal behavior in the system.

Heat transfer

To evaluate the heat transfer characteristics within the examined set-ups, we introduce the *global Nusselt numbers* corresponding to the two configurations, denoted as (VB) and (HB). These numbers are expressed as functions of the Reynolds number (Re), the volume fraction of hybrid nanofluid particles, ϕ, and the Richardson number values. The global Nusselt numbers associated with the (VB) and (HB) configurations, representing heat transfer across the vertical and horizontal blocks, are mathematically described by eqs. (20) and (22), respectively. These equations serve as crucial indicators of the heat transfer performance under varying conditions, allowing for a comprehensive analysis of the thermal behavior within the specified configurations.

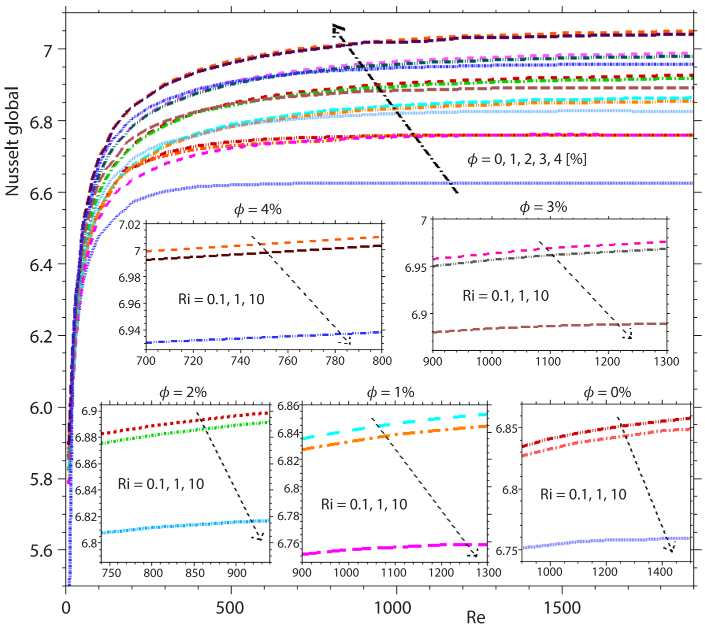

Figure 6. Variation of the global Nusselt number as a function of Reynolds number for VB configuration, for various values of Richardson number (0, 0.1, 10) and volume fraction of nanoparticles ϕ = 0-4%

The heat transfer of the VB configuration shown in fig. 6 was greater with the progressive increase in ϕ. Increasing Reynolds number brings the global Nusselt number to a constant value for all ϕ values.

Moreover, elevating the Reynolds number beyond Re > 500, under various Richardson number and hybrid nanofluid nanoparticle volume fraction, ϕ, results in only marginal improvements in heat transmission because the interaction between inertia and buoyancy effects is minimal.

Furthermore, as shown in fig. 7, when the Reynolds number remains within the range of Re ≤ 50 across a diverse set of Richardson numbers, the Nusselt number associated with hybrid nanofluids is observed to be inferior to that of uncontaminated water. This discrepancy can be attributed to a pronounced elevation in the dynamic viscosity of the nanofluids. This excessive increase in dynamic viscosity negatively impacts the heat transfer efficiency, resulting in lower Nusselt numbers compared to the baseline performance observed with pure water.

The alteration in the positioning of the heated block from the (VB) configuration the (HB) configuration led to a notable 51.16% enhancement in the heat transfer rate. This emphasizes the significant role played by geometric arrangements in influencing thermal dynamics.

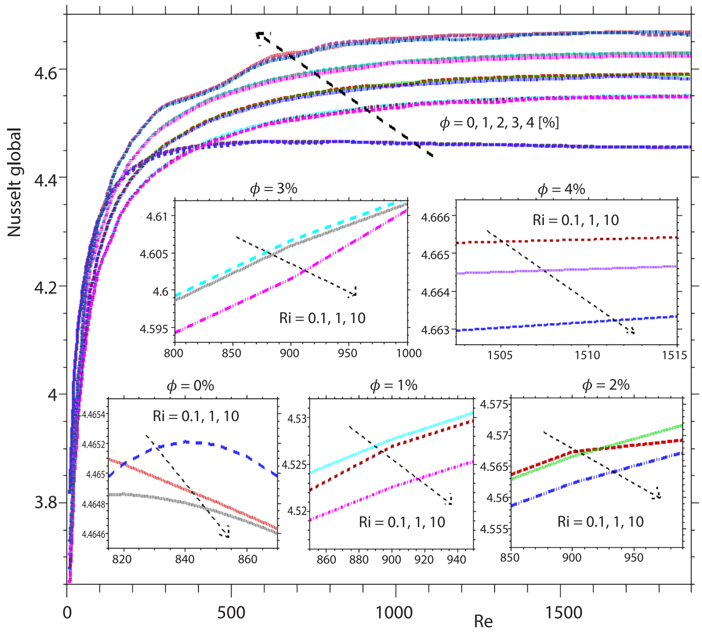

Figure 7. Variation of the global Nusselt number as a function of Reynolds number for HB configuration, for various values of Richardson number (0, 0.1, 10) and volume fraction of nanoparticles ϕ = 0-4%

Conclusions

Using the finite volume model and various leading factors such as the Reynolds number, Richardson number, and hybrid nanofluid (Cu-Al_2O_3) volume fraction of particles, a numerical study was conducted to examine *mixed convection* in a 3-D *L*-shaped chamber with an heated block for two considered configurations: (VB) and (HB). The main findings of this present investigation are as follows.

- For all Richardson numbers and for both configurations, the total Nusselt number increases with increasing Reynolds numbers and volume fraction of particles, except for the HB configuration when ϕ = 0% and Re > 840.
- For both configurations and for all volume fractions of nanoparticles, ϕ, increasing Re > 800 leads to a small variation in the heat transfer of less than 2% compared with when Re = 800.
- When Re ≤ 50 over a wide array of Richardson numbers, the Nusselt number of the hybrid nanofluids is lower than that of uncontaminated water, which can be referred to as an excessive increase in the dynamic viscosity.
- The isotherms and total Nusselt number revealed that the heat transfer in the VB configuration was better than that in the HB configuration. This may be explained by the fact that, in the HB configuration, the hybrid nanofluid speed decreases when it is deflected at the bottom of the cavity compared to the VB configuration.
- The heat transfer process was carried out by convection for all Reynolds numbers and particle volume fractions, as well as for all studied VB and HB configurations, and the Nusselt number values were nearly stable when the Richardson number was increased.
- When the heated block was repositioned from configuration (HB) to configuration (VB), heat transfer increased significantly by 51.16%, highlighting the importance of geometric arrangements in affecting thermal dynamics.

Nomenclature

A, B – dimensionless heat block, [–]
C_p – specific heat capacity, [JKg^{-1}K^{-1}]
Gr – Grashof number, [–]
g – gravitational hurrying, [ms^{-2}]
H – characteristic length, [m]
Ha – Hartman number, [–]
k – thermal conductivity", [Wm^{2}K^{-1}]
ℓ – dimensionless heat block, [–]
Nu – Nusselt number, [–]
P – pressure, [Pa]
Pr – Prandtl number, [–]
q'' – heat flux, [Wm^{-2}]
Re – Reynolds number, [–]
Ri – Richardson number, [–]
T – temperature, [K]
U, V, W – dimensionless velocity, [–]
X, Y, Z – dimensionless co-ordinates, [–]

Greek symbols

α – thermal diffusivity, [m^{2}s^{-1}]
β – coefficient of Thermal expansion, [K^{-1}]
μ – dynamic viscosity, [Kgm^{-1}s^{-1}]
ν – kinematic viscosity, [ms^{-1}]
ϕ – solid volume fraction of nanoparticles, [–]
θ – dimensionless temperature, [–]
ρ – density, [Kgm^{-3}]

Subscripts

c – cold
f – fluid
G – global
H – horizontal
hnf – hybrid-nanofluid
hnp – hybrid-nanoparticle
pi – considered particle
S – solid nanoparticlet
V – vertical

References

[1] Muhyaddin, J. H. R., *et al.*, Cooling a Cavity Equipped with a Hot Electrical Element Using Nanoencapsulated Phase Change Material/Water: Study of Mixed Convection And Natural-Convection, *Case Studies in Thermal Engineering*, *50* (2023), 103412
[2] Sheikholeslami, M., Ebrahimpour, Z., Thermal Improvement of Linear Fresnel Solar System Utilizing Al_2O_3-Water Nanofluid and Multi-Way Twisted Tape, *Int. J. Therm. Sci.*, *176* (2022), 107505
[3] Sannad, M., *et al.*, Effect of the Heating Block position on Natural-Convection in a 3-D Cavity Filled with Nanofluids, *Journal of Applied Fluid Mechanics*, *12* (2019), 1, pp. 281-291
[4] Doghmi, H., *et al.*, Effect of the Inlet Opening on Mixed Convection Inside a 3-D Ventilated Cavity, *Thermal Science*, *22* (2018), 6A, pp. 2413-2424
[5] Gangawane, K. M., Oztop, H. F., Mixed Convection in a Lid-Driven Cavity Containing Triangular Block with Constant Heat Flux: Effect Of Location Of Block, *Int. J. Mech. Sci.*, *152* (2019), Mar., pp. 492-511

[6] Asadi, A., *et al*., Heat Transfer Efficiency of Al_2O_3-MWCNT/Thermal Oil Hybrid Nanofluid as a Cooling Fluid in Thermal and Energy Management Applications: An Experimental and Theoretical Investigation, *Int. J. Heat Mass Transf*., *117* (2018), Feb., pp. 474-486

[7] Khalili, Z., Sheikholeslami, M., Investigation of Innovative Cooling System for Photovoltaic Solar Unit in Existence of Thermoelectric Layer Utilizing Hybrid Nanomaterial and Y-Shaped Fins, *Sustain. Cities Soc*., *93* (2023), 104543

[8] Rashad, A .M., *et al*., Entropy Generation and MHD Natural-Convection of Nanofluid in an Inclined Square Porous Cavity: Effects of a Heat Sink and Source Size and Location, *Chinese Journal of Physics 56* (2018), 1, pp. 193-211

[9] Mehmood, K., *et al.*, Numerical Simulation of MHD Mixed Convection in Alumina-Water Nanofluid Filled square porous cavity using KKL model: Effects of non-linear thermal radiation and inclined magnetic Field, *Journal of Molecular Liquids*, *238* (2017), pp, 485-498

[10] Armaghani, T., *et al.*, The MHD Mixed Convection of Localized Heat Source/Sink in an Al_2O_3-Cu-Water Hybrid Nanofluid in L-Shaped Cavity, *Alexandria Engineering Journal*, *60* (2021), 3, pp. 2947-2962

[11] Samrat, H., Swapan, K. P., Thermosolutal Hydromagnetic Mixed Convective Hybrid Nanofluid-Flow in a Wavy Walled Enclosure, *Journal of Magnetism and Magnetic Materials*, *572* (2023), 15, 170580

[12] Patankar, S. V., *Numerical Heat Transfer And Fluid-Flow,* McGraw-Hill,. New York., USA, 1980

[13] Ravnik, J., Analysis of 3-D Natural-Convection of Nanofluids by BEM, Engineering Analysis with Boundary Elements, *Engineering Analysis with Boundary Elements*, *34* (2010), 12, pp. 1018-1030

[14] Iwatsu, R., *et al*., Mixed Convection in a Driven Cavity with a Stable Vertical Temperature Gradient, *Int. J.Heat Mass Transf.*, *36* (1993), 6, pp. 1601-1608

[15] Khanafer, K., Chamkha, A. J., Mixed Convection Flow in a Lid Driven Enclosure Filled with a Fluid-Saturated Porous Medium, *Int. J. Heat Mass Transf*., *42* (1999), 13, pp. 2465-2481

[16] Gorla, R. S. R., *et al*., Heat Source/ Sink Effects on a Hybrid Nanofluid-Filled Porous Cavity, *Journal Thermophys. Heat Transf*., *31* (2017), 4, pp. 847-857

Paper submitted: September 16, 2023
Paper revised: November 30, 2023
Paper accepted: December 28, 2023